Magnetic force microscopy of ferromagnetic nanoparticles formed in Al_2O_3 and SiO_2 by ion implantation

C. E. Vallet,[a] C. W. White, S. P. Withrow, J. D. Budai, and L. A. Boatner
Oak Ridge National Laboratory, Oak Ridge, Tennessee 37831

K. D. Sorge
The University of Tennessee, Knoxville, Tennessee 37996

J. R. Thompson
Oak Ridge National Laboratory, Oak Ridge, Tennessee 37831 and The University of Tennessee, Knoxville, Tennessee 37996

K. S. Beaty and A. Meldrum
Department of Physics, The University of Alberta, Edmonton, Alberta T6G 2J1, Canada

(Received 26 June 2002; accepted 12 August 2002)

Magnetic force microscopy (MFM) has been used to investigate the properties of ferromagnetic FePt nanoparticles produced by the implantation of Fe and Pt ions into single-crystal Al_2O_3 or fused SiO_2 followed by thermal processing. The MFM results are compared to cross-section and plan view transmission electron microscopy images of the same samples. We demonstrate that MFM can detect magnetism in nanosized particles that are situated several hundred nm below the sample surface. MFM is shown to be a promising tool for studying the characteristics of magnetic nanoparticles produced by ion implantation. © *2002 American Institute of Physics.*
[DOI: 10.1063/1.1512693]

I. INTRODUCTION

The production of magnetic nanoparticles with a controlled particulate size is currently of significant technological interest. An increasing number of applications of materials of this type include ultrahigh-density magnetic recording materials,[1] magnetooptically active nanocomposites,[2] and nanoparticle fluids with applications in both medical imaging[3] and drug delivery.[4]

Magnetic force microscopy (MFM), from its inception, has been widely used to study magnetism on the nanoscale for a variety of systems ranging from thin-film surfaces to biological samples.[5–7] The principles of the method are discussed in detail in several review articles.[8,9] MFM has also been used to study the magnetic properties of two-dimensional nanoparticle arrays[10,11] and of nanoparticle assemblies in thin films.[12–15] Samples produced by the shallow implantation of Fe into amorphous SiO_2 films followed by annealing in N_2 have also been studied using both atomic force microscopy and MFM.[16] These latter results were obtained for composites in which the magnetic phase was situated at the sample surface, and the magnetic images could be directly correlated with the specimen topography.

In the work reported here, we have used magnetic force microscopy to study ferromagnetic FePt nanoparticles encapsulated in the near surface of Al_2O_3 or fused SiO_2 matrices. These nanoparticles are produced by the sequential implantation of Fe and Pt followed by thermal annealing. The FePt nanoparticles synthesized in this process are in the chemically ordered $L1_0$ phase, and they exhibit extremely high magnetic coercivities (greater than 20 kOe at low temperatures).[17] In the case of implantation into Al_2O_3, by controlling the implantation temperature we have produced either large or small nanoparticles of FePt. MFM images are presented from samples containing these microstructures. For the case of FePt particles precipitated in an SiO_2 host, MFM images are shown for a sample with embedded nanoparticles as large as 70 nm in diameter. For all of the implanted samples, images of the topography of micron-sized areas are obtained sequentially with the magnetic force images that were obtained by using phase detection. The MFM results are also compared to transmission electron microscope (TEM) micrographs[17] that provide indications of the physical size and spatial distribution of the embedded particles. Magnetic force microscopy was able to detect nanosized ferromagnetic particles located several hundred nanometers below the surface. A comparison with TEM images confirmed that the particles observed by TEM are ferromagnetic.

II. EXPERIMENT

FePt nanoparticles were formed using the sequential ion implantation of Fe (350 keV, 1×10^{17} cm^{-2}) and Pt (910 keV, 8.2×10^{16} cm^{-2}) into single-crystal α-Al_2O_3 or amorphous SiO_2, followed by thermal annealing. These implantation conditions lead to overlapping Fe/Pt profiles centered at a depth of ~160 nm in Al_2O_3 and ~260 nm in SiO_2. For the case of single-crystal α-Al_2O_3, the implantation was carried out either at high temperature (550 °C for Fe and 500 °C for Pt), or at a somewhat lower temperature (200 °C for each

[a]Author to whom correspondence should be addressed; electronic mail: valletce@ornl.gov

 © 2002 American Institute of Physics

Downloaded 11 Sep 2009 to 160.91.157.167. Redistribution subject to AIP license or copyright; see http://jap.aip.org/jap/copyright.jsp

species). The implanted samples were annealed at 1100 °C for 2 h in flowing Ar+4%H_2. Annealing is necessary to remove lattice damage induced by the ion implantation process and to precipitate the chemically ordered $L1_0$ phase of FePt. Our previous work[17] has established that small FePt nanoparticles (2–10 nm diameter with a few particles as large as 25 nm diameter) are produced by implantation at the higher temperatures, whereas very large particles up to 2 μm long in a thin layer parallel to the surface result from the 200 °C implantation. Hence, the size of the nanoparticles can be altered dramatically without changing the total implant doses or the alloy composition. For the case of the SiO_2 host, the Fe and Pt ions were implanted only at the higher temperatures, and the samples were annealed at 1000 °C for 2 h in flowing Ar+4% H_2. Assuming complete alloying, the particles formed in both the Al_2O_3 and SiO_2 hosts have the Fe-rich composition $Fe_{55}Pt_{45}$.

A magnetic force microscope (Digital Instruments NanoScope III MultiMode) was used to obtain surface topography images as well as to locate the FePt particles below the sample surface. The topography and magnetic images were obtained sequentially. A line scan was first taken with the tip oscillating at its resonant frequency and establishing intermittent contacts with the surface [tapping mode (TM)] to obtain an image of the surface features. Then, the same scan was repeated in the same direction with the tip lifted from the surface by a selected constant distance (lift mode) to generate a magnetic-force image. Standard etched silicon tips covered with a thin magnetic coating (MESP from Digital Instruments) were used. The resonance frequency of the free oscillating tips was ~63 kHz. The tip was magnetized along its axis, i.e., during recording, the tip magnetic field was perpendicular to the inspected surface. While surveying magnetic material, the tip oscillating frequency was shifted by an amount proportional to the vertical gradients in the magnetic forces exerted on the tip.[18] The small frequency shifts were detected through corresponding phase shifts. Consequently, each raster of a magnetic image detects magnetic material that is confined in a volume perpendicular to the surface directly below the tip. In this sense, the magnetic image directly mimics a plan-view TEM image of magnetic particles embedded in the substrate. For selected samples, additional topography images were obtained in the tapping mode with a nonmagnetic tip and by using the contact mode technique in which the tip was in constant contact with the surface.

III. RESULTS

A. α-Al_2O_3 implanted at 200 °C

Plan-view and cross-section TEM micrographs from Al_2O_3 implanted at 200 °C and then annealed are shown in Fig. 1. Large FePt particles up to 2 μm long in a thin layer (~50 nm thick) are located about 150 nm from the surface.[17] The depth of these particles corresponds to the peak of the implanted-ion distribution profiles for the implant conditions of the Fe and Pt. In addition to the large particles, much smaller nanosized particles formed at a depth of ~250 nm, which corresponds to the implantation end-of-range. X-ray diffraction results indicate that at least some of the FePt is oriented with its ⟨111⟩ axis directed along the *c* axis (normal axis) of the Al_2O_3 host crystal. Magnetic measurements show that the particles are ferromagnetic with a magnetic coercivity of ~23 kOe at 5 K and ~17 kOe at 300 K.

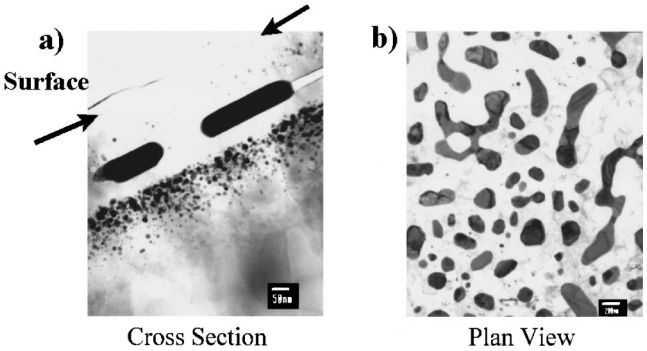

FIG. 1. (a) Cross-section and (b) plan-view TEM images of annealed α-Al_2O_3 implanted at 200 °C with Fe(350 keV, $1\times10^{17}/cm^2$) and Pt(910 keV, $8.2\times10^{16}/cm^2$). The scale bar on the cross-section view (left) is 50 nm, and that on the plan view (right) is 200 nm.

Magnetic images obtained by scanning the surface of the sample used in Fig. 1 are presented in Fig. 2. Results are given for 2 μm×2 μm scans for lift heights ranging from 25 to 250 nm. The images were obtained after magnetization of the sample in a magnetic field of 65 kOe that was applied normal to the sample surface. The phase scale is 0°–1°. Dark areas in these images correspond to the detection of magnetic signals from the FePt particles. The image recorded at the closets tip separation from the surface, 25 nm, exhibits rather

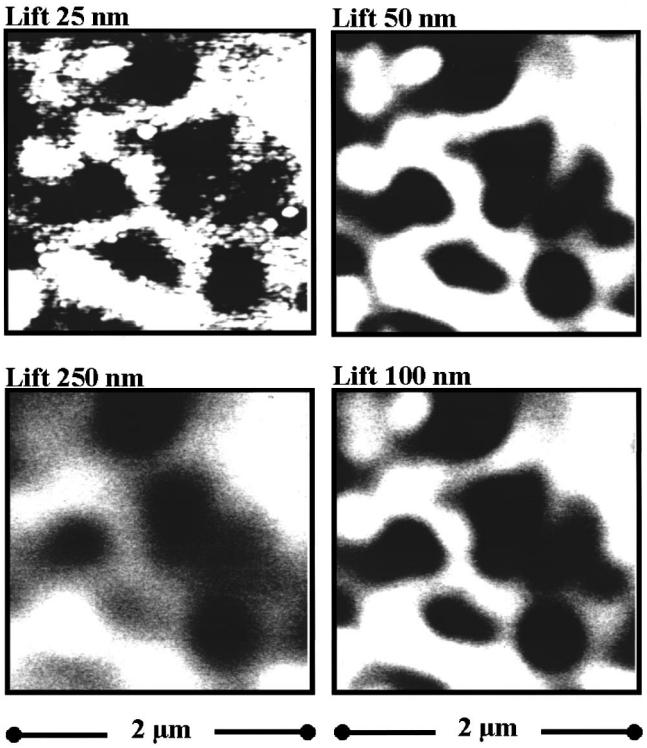

FIG. 2. Effect of tip/surface separation on magnetic force images. Annealed α-Al_2O_3 implanted at 200 °C with Fe (350 keV, $1\times10^{17}/cm^2$) and Pt (910 keV, $8.2\times10^{16}/cm^2$). Magnetic images were taken with tip/surface separations of 25, 50, 100, and 250 nm and are shown on a 0°–1° phase scale.

Downloaded 11 Sep 2009 to 160.91.157.167. Redistribution subject to AIP license or copyright; see http://jap.aip.org/jap/copyright.jsp

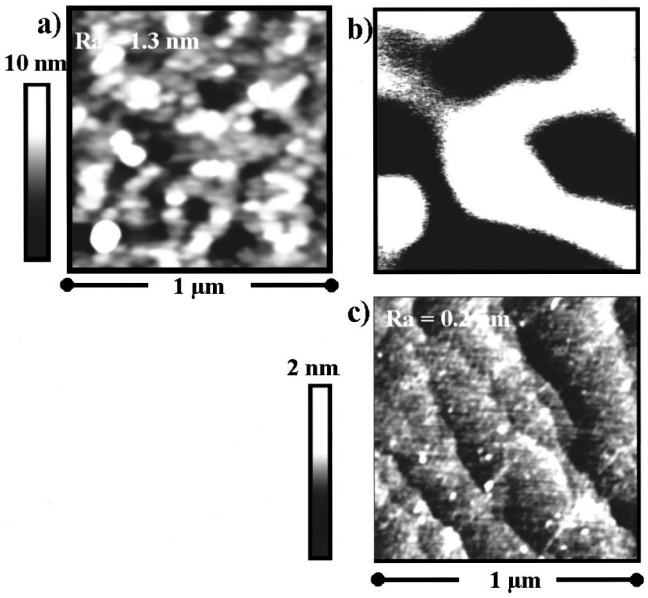

FIG. 3. (a) Topography (TM) of a (1 μm×1 μm) area on a 0–10 nm height scale of α-Al_2O_3 implanted at 200 °C with Fe (350 keV, $1\times10^{17}/cm^2$) and Pt (910 keV, $8.2\times10^{16}/cm^2$), annealed at 1100 °C in Ar+4%H_2 and magnetized in a 65 kOe field normal to the surface; (b) Magnetic (phase) image obtained sequentially with (a) on a 0°–1° phase scale. Lift height was 50 nm for magnetic imaging; (c) Topography (TM) of a (1 μm×1 μm) unimplanted area of the annealed sample with a 0–2 nm height scale.

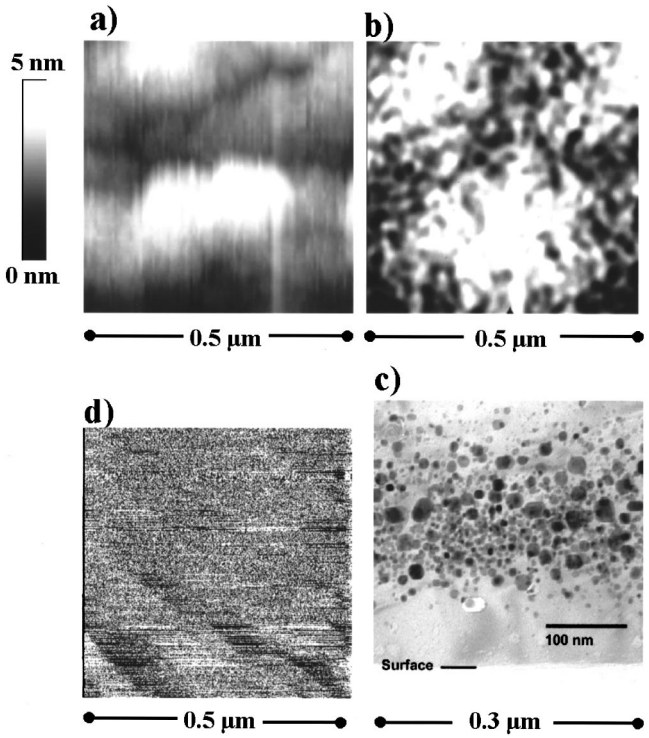

FIG. 4. (a)–(d) clockwise: α-Al_2O_3 (0001) implanted with Fe (350 keV, $1\times10^{17}/cm^2$, 550 °C) and Pt (910 keV, $8.2\times10^{16}/cm^2$, 500 °C). Sample was magnetized along the *c* axis in a 65 kOe field after annealing at 1100 °C in Ar+4%H_2. (a) TM topography of (0.5 μm×0.5 μm) area on a 0–5 nm height scale; (b) Magnetic image of the same area as (a) on a 0°–0.3° phase scale; (c) Cross-section TEM image; and (d) Magnetic image of unimplanted α-Al_2O_3 on a 0°–2° phase scale obtained with a lift height of 5 nm.

mottled features on the order of 7–10 nm that are superimposed on much larger areas of strong light/dark contrast. By comparison to the surface topography [see the image in Fig. 3(a)], the small granular regions correspond to topographical features whereas the dark/light features are due to detection of the magnetic signal. For lift heights from 50 to 250 nm, the magnetic images retain the large dark/light regions but are free from topographic features. However, the images become increasingly blurred as the tip/surface separation is increased and, therefore, may overestimate the area of magnetic material. These results indicate that for this sample lift heights greater than ~50 nm from the surface are suitable for detecting magnetic signals that are free from the topological features of this sample. It should be noted that the necessary separation to detect magnetic phases independent of topography is highly dependent on the depth and magnetic nature of the particles.

Tapping mode and magnetic images from the same 1 μm×1 μm surface area of a 200 °C-implanted Al_2O_3 sample are shown in Figs. 3(a) and 3(b). For comparison, a TM scan of an unimplanted area of the same Al_2O_3 sample is also given in Fig. 3(c). The image of the unimplanted area shows a terrace/step morphology that may indicate a small miscut along the Al_2O_3 [001] face.[19] The unimplanted surface has an average roughness of 0.2 nm. The tip used for obtaining the image shown in Fig. 3(c) was a sharp NanoDevices TAP300 that is nonmagnetic and has a resonance frequency of about 260 kHz. This probe produces a sharper image than the tips coated with a magnetic oxide that were used for the TM and MFM images in Figs. 3(a) and 3(b).

After implantation and annealing, the surface topography changes considerably as seen in the TM image of Fig. 3(a) on a 0–10 nm height scale. A roughening of the surface is indicated by the contrasting small light and dark areas. The average mean roughness of the implanted surface is 1–1.5 nm. In addition, some surface contamination is likely to be present as indicated by the bright white areas.

The magnetic phase image shown in Fig. 3(b), obtained with a lift height of 50 nm, is from the same area as the TM image of Fig. 3(a). No indication of the topography remains at this lift height. On the other hand, the network of dark features can be directly correlated with the FePt particles observed in the plan-view micrograph of Fig. 1(b). The features are on the same scale and have the same disconnected morphology. Hence, it can be concluded that MFM is capable of detecting magnetic particles formed well below the surface.

B. α-Al_2O_3 implanted at 550/500 °C

Tapping-mode and lift-mode images from 0.5 μm×0.5 μm areas of a sample implanted at high temperature are given in Figs. 4(a) and 4(b), respectively. The measured roughness of the implanted surface is ~1.7 nm—slightly more than that seen for the case of implantation at 200 °C. The magnetic image was recorded on a 0°–0.3° scale with a lift height of 80 nm. Although the contrast in the magnetic image is partially correlated to the topography due to charging at the surface, many small darker spots appear over both the light and dark regions. These are an indication of mag-

Downloaded 11 Sep 2009 to 160.91.157.167. Redistribution subject to AIP license or copyright; see http://jap.aip.org/jap/copyright.jsp

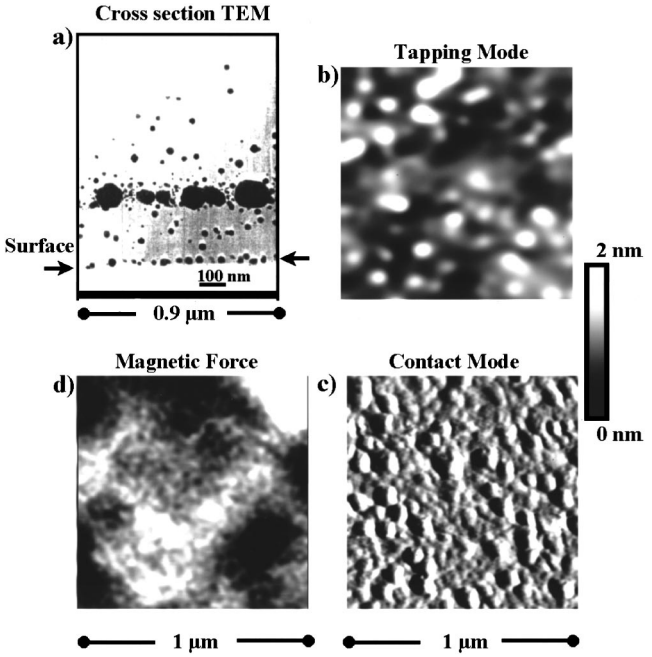

FIG. 5. (a)–(d) clockwise: SiO_2 implanted with Fe (350 keV, $1\times10^{17}/cm^2$, 550 °C) and Pt (910 keV, $8.2\times10^{16}/cm^2$, 500 °C) and magnetized in a 65 kOe field after annealing in $Ar+4\%H_2$. (a) Cross section TEM image; (b) TM topography of (1 μm×1 μm) area on a 0–2 nm height scale; (c) Topography of a (1 μm×1 μm) area obtained using the contact mode shown with same height scale of 0–2 nm as (b); and (d) Magnetic force image obtained sequentially with (b) on a 0°–0.5° phase scale with a lift height of 100 nm.

netic interaction. The pattern of the magnetic signal in Fig. 4(b) is considerably different than that seen for the lower-temperature implant in Fig. 3(c). A cross-section TEM micrograph from the sample implanted at high temperature is given in Fig. 4(c), and this image shows discrete FePt nanoparticles with sizes on the order of 10–20 nm that are located ~100 nm or more below the surface. The magnetic structure seen in Fig. 4(b) is comparable in size to the spherical particles observed in the cross-section TEM image. A very different magnetic image, shown in Fig. 4(d), was obtained for an unimplanted α-Al_2O_3 sample with a magnetized tip surveying at an even closer distance, 5 nm, from the surface. In Fig. 4(d) no features attributable to magnetic signals are seen. These results suggest that MFM using a standard tip is capable of detecting particles with high coercivity as small as a few tens of nm in diameter.

C. SiO_2 implanted at 500–550 °C

FePt nanoparticles have also been formed in SiO_2 by implantation and annealing. A cross-section TEM micrograph, shown in Fig. 5(a), indicates that the FePt alloy particles are nearly spherical and have a bimodal size distribution, with small particles near or at the surface and larger particles situated at a depth of about 250 nm from the surface. The size of the smaller particles is ~2–10 nm, which is comparable to the resolution limit of a standard magnetic tip. The larger particles in the TEM image have diameters on the order of 60–80 nm. X-ray diffraction data demonstrate that these nanoparticles are randomly oriented.[17] The nanoparticles have a magnetic coercivity in excess of 30 kOe. The tapping-mode and contact-mode images presented in Figs. 5(b) and 5(c) show the surface topography from a 1 μm square of an ion-implanted fused SiO_2 substrate. The contact-mode image was obtained using a standard Digital Instruments Si_3N_4 tip that is in contact with the surface at all points. The measured surface mean roughness is on the order of 0.3 nm for the results shown in both Figs. 5(b) and 5(c). A contact-mode image from unimplanted SiO_2 (not shown) is very similar to that seen after processing, indicating that the implantation and thermal anneal has not significantly altered the topography. This suggests that the small particles close to the surface don't break through the surface as was the case reported in Ref. 16. A MFM image obtained from the same area as the TM image is shown in Fig. 5(d). The magnetic interaction between the tip and surface was somewhat weak, and the lift height was fixed at 100 nm in order to obtain contrasted MFM images on a 0°–0.5° scale. Both large areas of magnetic signal as well as much smaller regions of magnetic interaction distributed over the whole image can be seen in Fig. 5(d). The features in the magnetic image correlate with both the large and small particles seen by TEM. The magnetic interaction from the small particles appears to be less than that exerted by the embedded larger particles, but similar to that observed in α-Al_2O_3 implanted at 550/500 °C [Fig. 4(b)] which contains small nanoparticles of FePt. The MFM measurements confirm that the implant and annealing conditions were adequate to produce ferromagnetic phase(s) of FePt in SiO_2. Very likely, the overall magnetic properties of the sample are dominated by the large $Fe_{55}Pt_{45}$ particles. The results presented here provide information regarding the formation, morphology, and location of magnetic phases. This information, in turn, provides an increased understanding of the effects of annealing on the formation of magnetic FePt nanoparticles in ion-implanted SiO_2 samples.

IV. CONCLUSION

Magnetic force microscopy has been utilized to detect magnetic FePt nanoparticles that were formed in Al_2O_3 and SiO_2 by ion implantation followed by annealing and subsequently magnetized perpendicular to the sample surface. Small particles, on the order of a few tens of nm near the surface, and larger particles buried up to ~250 nm below the surface have been imaged. The identification of the FePt alloy phase has been confirmed by comparison to TEM results. A major advantage of the MFM technique is that it is nondestructive. Improvements in the sharpness of the magnetic probes and observations under in-plane magnetic fields should lead to a more detailed analysis of the magnetic properties of nanoparticles formed by ion-beam methods.[20,21]

ACKNOWLEDGMENTS

This research was sponsored by the Division of Materials Sciences, Office of Basic Energy Sciences, U.S. Department of Energy under Contract No. DE-AC05-00OR22725. Oak Ridge National Laboratory is managed and operated by UT-Battelle, LLC.

Downloaded 11 Sep 2009 to 160.91.157.167. Redistribution subject to AIP license or copyright; see http://jap.aip.org/jap/copyright.jsp

[1] S. Sun, C. B. Murray, D. Weller, L. Folks, and A. Moser, Science **287**, 1989 (2000).
[2] S. Honda, F. A. Modine, A. Meldrum, J. D. Budai, T. E. Haynes, and L. A. Boatner, Appl. Phys. Lett. **77**, 711 (2000).
[3] R. Weissleder *et al.*, Radiology **175**, 489 (1990); L. Josephson *et al.*, Bioconjugate Chem. **10**, 186 (1999).
[4] L. Brannon-Peppas, *Medical Plastics and Biomaterials Magazine*, November/December (Canon Communications LLC, Los Angeles, 1997).
[5] Y. Martin and H. K. Wickramasinghe, Appl. Phys. Lett. **50**, 1455 (1987).
[6] P. Grütter, H. J. Mamin, and D. Rugar, in *Scanning Tunneling Microscopy*, edited by R. Wiesendanger and H.-J. Güntherodt (Springer, Heidelberg, 1992), Vol. II, p. 151.
[7] R. Proksch, T. E. Schäffer, B. M. Moskowitz, E. D. Dahlberg, D. A. Bazylinski, and R. B. Frankel, Appl. Phys. Lett. **66**, 2582 (1995).
[8] S. Porthun, L. Abelmann, and C. Lodder, J. Magn. Magn. Mater. **182**, 238 (1998).
[9] U. Hartmann, Annu. Rev. Mater. Sci. **29**, 53 (1999).
[10] M. Hwang, M. C. Abraham, T. A. Savas, H. I. Smith, R. J. Ram, and C. A. Ross, J. Appl. Phys. **87**, 5108 (2000).
[11] M. Hanson, C. Johansson, B. Nilsson, P. Isberg, and R. Wäppling, J. Appl. Phys. **85**, 2793 (1999).
[12] I.-S. Lee and D.-W. Kim, Thin Solid Films **388**, 245 (2001).
[13] C. P. Luo, S. H. Liou, and D. J. Sellmyer, J. Appl. Phys. **87**, 6941 (2000).
[14] Y. Samson, A. Marty, R. Hoffman, V. Gehanno, and B. Gilles, J. Appl. Phys. **85**, 4604 (1999).
[15] T. Suzuki, N. Honda, and K. Ouchi, J. Appl. Phys. **85**, 4301 (1999).
[16] X.-z. Ding, B. K. Tay, X. Shi, M. F. Chiah, W. Y. Cheung, S. P. Wong, J. B. Xu, and I. H. Wilson, J. Appl. Phys. **88**, 2745 (2000); X.-z. Ding, M. F. Chiah, W. Y. Cheung, S. P. Wong, J. B. Xu, I. H. Wilson, H.-m. Wang, L.-z. Chen, and X.-h. Liu, *ibid.* **86**, 2550 (1999).
[17] C. W. White, S. P. Withrow, J. D. Budai, L. A. Boatner, K. D. Sorge, J. R. Thompson, K. S. Beaty, and A. Meldrum, Nucl. Instrum. Methods Phys. Res. B **191**, 437 (2002).
[18] R. D. Gomez, E. R. Burke, and I. D. Mayergoyz, J. Appl. Phys. **79**, 6441 (1996).
[19] C. E. Vallet, C. S. Prouteau, R. Feenstra, J. F. Hamet, D. T. Verebelyi, and D. K. Christen, Surf. Interface Anal. **29**, 221 (2000).
[20] R. D. Gomez, M. C. Shih, R. M. H. New, R. F. W. Pease, and R. L. White, J. Appl. Phys. **80**, 342 (1996).
[21] P. Vavassori, O. Donzelli, V. Metlushko, M. Grimsditch, B. Ilic, P. Neuzil, and R. Kumar, J. Appl. Phys. **88**, 999 (2000).

Downloaded 11 Sep 2009 to 160.91.157.167. Redistribution subject to AIP license or copyright; see http://jap.aip.org/jap/copyright.jsp